Geosci. Model Dev. Discuss., 5, 3217–3260, 2012
www.geosci-model-dev-discuss.net/5/3217/2012/
doi:10.5194/gmdd-5-3217-2012

Geoscientific Model Development Discussions

Implementation of the Fast-JX Photolysis scheme into the UKCA component of the MetUM chemistry climate model

P. J. Telford[1,2], N. L. Abraham[1,2], A. T. Archibald[1,2], P. Braesicke[1,2], M. Dalvi[3], O. Morgenstern[4], F. M. O'Connor[3], N. A. D. Richards[5], and J. A. Pyle[1,2]

[1]NCAS Climate, University of Cambridge, Cambridge CB2 1EW, UK
[2]Centre for Atmospheric Science, Department of Chemistry, University of Cambridge, Cambridge CB2 1EW, UK
[3]Met Office Hadley Centre, Exeter, UK
[4]National Institute of Water and Atmospheric Research, Lauder, New Zealand
[5]Institute for Climate and Atmospheric Science, School of Earth and Environment, University of Leeds, UK

Received: 3 October 2012 – Accepted: 9 October 2012 – Published: 17 October 2012

Correspondence to: P. J. Telford (paul.telford@atm.ch.cam.ac.uk)

Published by Copernicus Publications on behalf of the European Geosciences Union.

Abstract

Atmospheric chemistry is driven by photolytic reactions, making their modelling a crucial component of atmospheric models. We describe the implementation and validation of Fast-JX, a state of the art model of interactive photolysis, into the MetUM chemistry climate model. This allows for interactive photolysis frequencies to be calculated in the troposphere and augments the calculation of the frequencies in the stratosphere by accounting for clouds and aerosols in addition to ozone. In order to demonstrate the effectiveness of this new photolysis scheme we employ new methods of validating the model, including techniques for sampling the model to compare to flight track and satellite data.

1 Introduction

In the recent past efficient comprehensive photolysis schemes have been developed that are fast enough to be run within global, three dimensional models, allowing a more interactive treatment of photolysis frequencies in composition modelling (Wild et al., 2000; Tie et al., 2003). These have been implemented into a range of global, three dimensional models (see for instance Liu et al., 2006; Voulgarakis et al., 2009) and have been demonstrated to provide an improved description of atmospheric composition, especially in regions where photolysis and variations in optical depth are important.

The UKCA module is a component of the UK Met Office's Unified Model (MetUM). A number of model configurations have been established and tested; one with stratospheric chemistry (Morgenstern et al., 2009), one with tropospheric chemistry (O'Connor et al., 2009; Telford et al., 2010)[1] and one with the GLOMAP-mode aerosol scheme (Mann et al., 2010). There are also whole atmosphere chemistry schemes that have been developed from the tropospheric and stratospheric chemistries (Archibald

[1] A more detailed description is in preparation by F. M. O'Connor et al.

GMDD
5, 3217–3260, 2012

et al., 2012; Morgenstern et al., 2012). We describe the addition of the Fast-JX photolysis code into the MetUM framework and evaluate it against a range of observations.

Although we make some comparisons in an idealised atmosphere based on the CCMVal model intercomparison (Chipperfield et al., 2010), the main evaluation here is carried out using a "nudged" tropospheric model simulation from 2004 through to 2008. The technique of nudging constrains the model to meteorological re-analyses, allowing the model to reproduce the observed weather (Telford et al., 2008). This allows us to make comparisons with an expanded range of data-sets, including those from campaigns and from satellites. Although most of our validation is performed on the tropospheric model, as this is where the interactive photolysis is more important because of the effects of clouds, we also include a short section on the performance of the stratospheric model.

2 Model description

The UKCA chemistry module is part of the Met Office's Unified Model (MetUM). We employ a version of the model based on the HadGEM3 configuration (Hewitt et al., 2011), but with the following configuration:

- a horizontal resolution of 3.75° × 2.5° in longitude and latitude.
- 60 hybrid height levels in the vertical, from the surface up to a height of 84 km.

A time series of sea surface temperatures and sea ice coverage are prescribed from the HadISST dataset (Rayner et al., 2003).

2.1 Nudging

The technique of nudging is used to reproduce the atmospheric conditions over the period studied. The nudging is applied from 3 to 45 km with a relaxation time scale of 6 h (Telford et al., 2008). For the first time we nudge to the ERA-Interim re-analysis

GMDD
5, 3217–3260, 2012

data (Dee et al., 2011) instead of the ERA-40 re-analyses. These are the latest re-analysis products from the ECMWF with the following changes from the ERA-40 re-analysis: higher horizontal resolution, 4D-var data assimilation, new humidity analyses, and improved model physics, and a different period of coverage (1979–2012 compared to 1957–2002 in ERA-40).

2.2 Tropospheric chemistry

The tropospheric version of the model employs a medium sized chemistry scheme that simulates the O_x, HO_x and NO_x chemical cycles and the oxidation of CO, ethane, propane, and isoprene (Telford et al., 2010). The Mainz isoprene mechanism (Pöschl et al., 2000) is used to parameterise isoprene oxidation. In total the model has 168 chemical reactions and 56 chemical tracers. We also add the reaction between HO_2 and NO using the rates and yields of Butkovskaya et al. (2007) and hydrolysis of N_2O_5 (Morgenstern et al., 2009). Concentrations of ozone and NO_y are overwritten above 30 hPa. The upper boundary condition for NO_y are taken from the Cambridge 2-D model (Law and Pyle, 1993a,b). The upper boundary conditions for O_3 are taken from the Rosenlof climatology (Dall'Amico et al., 2010). Methane is fixed to 1.76 ppmv throughout the atmosphere. Dry deposition and wet deposition are parameterised using the approaches of Giannakopoulos et al. (1999).

Seven chemical species (nitrogen oxide (NO), carbon monoxide (CO), formaldehyde (HCHO), ethane, propane, acetaldehyde and acetone ($(CH_3)_2CO$)) are emitted in the manner of Zeng and Pyle (2003). Isoprene (C_5H_8) emissions are included in a similar manner, though with a diurnal cycle as in Young (2007). The emissions are taken from a sum of anthropogenic and natural emissions, with anthropogenic and biomass burning emissions taken from Lamarque et al. (2010) using data for the year 2000. We also lump the emissions of ethene and ethyne with ethane, and propene with propane. Aircraft emissions of NO are taken from Eyers et al. (2004). We also include biogenic emissions of CO, Me_2CO and C_5H_8 and emissions of NO from natural soil emissions and lightning. The biogenic emissions are distributed according to Guenther et al.

GMDD
5, 3217–3260, 2012

(1995) and total 40 $Tg yr^{-1}$ of CO from the oceans and 45 $Tg yr^{-1}$ of CO, 40 $Tg yr^{-1}$ of Me_2CO and 570 $Tg yr^{-1}$ of C_5H_8 from the land. We include, on average, 5 $Tg yr^{-1}$ of lightning emissions distributed according to the parameterisation of Price and Rind (1994). Finally we include 5.6 $Tg yr^{-1}$ of NO_x from natural soil emissions distributed according to the empirical model of Yienger and Levy II (1995).

2.3 Stratospheric chemistry

The stratospheric version of the model has a comprehensive stratospheric chemistry, including chlorine and bromine chemistry, heterogeneous processes on polar stratospheric clouds (PSCs), and liquid sulphate aerosols as well as a simplified tropospheric chemistry (Morgenstern et al., 2009). More detailed descriptions of the stratospheric version of the chemistry can be found in Morgenstern et al. (2009).

There are a few differences between the stratospheric model used in this study and that in Morgenstern et al. (2009). The base version of the climate model has been updated to HadGEM3 from HadGEM1a. In addition N_2O is now transported completely separately from the other odd nitrogen species and the reaction $N_2O + O(^1D)$ has been updated with rates from a more recent JPL assessment (Sander et al., 2006).

2.4 Climatological photolysis schemes

In earlier versions of the model, photolysis frequencies were determined from frequencies calculated off-line under average conditions, tabulated and interpolated for use on-line. There were two schemes, one for use in the troposphere, and one for use in the stratosphere. The tropospheric configuration of the chemistry model exclusively used the tropospheric photolysis scheme. The stratospheric configuration of the chemistry model used the tropospheric photolysis scheme below 300 hPa, the stratospheric photolysis scheme above 200 hPa with a linear transition between the two schemes from 200 hPa and 300 hPa.

GMDD
5, 3217–3260, 2012

The tropospheric photolysis scheme employed the two stream method of Hough (1988) with clouds included as a zonally averaged climatological distribution (Law et al., 1998). The photolysis frequencies depended only on latitude, local solar time, month of the year and pressure. The stratospheric scheme was based on the look up table approach of Lary and Pyle (1991), with some updated cross section measurements (Morgenstern et al., 2009). The frequencies in the stratospheric scheme responded to changes in the overhead ozone column.

Apart from the stratospheric ozone, these schemes did not respond to changes in optical depth, relying instead on average conditions for particular latitudes and altitudes. This precluded us from looking at a complete set of feedbacks caused by variations in the optical depth (from e.g. clouds, aerosols) onto atmospheric composition, limiting our ability to simulate the atmosphere. The addition of a more complete interactive photolysis scheme allows us to overcome this hurdle.

2.5 Fast-J interactive photolysis schemes

Recently photolysis schemes suitable for interactive use, including the Fast-J scheme, have been developed that are fast enough to be incorporated into global models. The original Fast-J scheme was developed for tropospheric photochemistry (Wild et al., 2000). It arranged light from wavelengths between 289 to 850 nm into seven discrete bins. A further development, Fast-J2, extended the scheme into the stratosphere (Bian and Prather, 2002) by adding 11 wavelength bins from 177–290 nm. To speed up the code the rayleigh scattering for the additional wavelengths was treated as pseudo absorption. In the absence of this scattering Fast-J2 fails to reproduce stratospheric photolysis frequencies at low solar zenith angles or at dusk, yielding problems in the high latitude winter stratosphere (Morgenstern et al., 2009) and has difficulties in describing the effects of high aerosol loadings. Fast-JX combines these two schemes, providing the full scattering calculation for all 18 wavelength bins (Neu et al., 2007). It also has several other improvements most notably a more efficient way of introducing extra

GMDD
5, 3217–3260, 2012

levels for very optically dense clouds. It is the implementation of this code into the MetUM model that we describe.

3 Technical implementation

We take the Fast-JX code from the Fast-JX website[2], this will now be referred to as Prather et al. (2010). Given the optical depth from absorbing and scattering species this code determines how many photons of each wavelength are absorbed and scattered as light passes through the atmosphere.

This is done using the "plane parallel assumption" which assumes that, for a grid box, the horizontal properties are constant and radiative transfer properties only depend on the vertical co-ordinate. Radiative fluxes between horizontally adjacent grid-boxes is also neglected. The calculation of the radiative properties thus divides into a series of columns. The path of the radiation is traced through this column, being scattered or absorbed according to the contents of the grid-box. The amount of scattering and absorption depends on the optical depth of the different scatterers in the grid-box.

The photolysis frequencies ("j" rates) for each reaction are determined from the wavelength bin resolved flux in each grid-box and the cross section of each species in each wavelength bin. These cross sections are evaluated from experimental measurements of the frequencies as described in Sect. 3.2. Because Fast-JX still does not provide photolysis frequencies for wavelengths below 177 nm, which are important for some reactions in the upper stratosphere and mesosphere we evaluate the cross sections for these wavelengths using the original climatological scheme Lary and Pyle (1991) and add them to the Fast-JX reaction frequencies. For speed this extra calculation is only performed above 20 Pa as below this level the flux of these high energy photons is negligible.

[2] http://www.ess.uci.edu/~prather/fastJX.html (version 6.4)

GMDD
5, 3217–3260, 2012

3.1 Calculation of optical depth

The optical depth (τ) is determined as the sum of the optical depth of ice water clouds (τ_w), liquid water clouds (τ_i), aerosols, ozone and oxygen and rayleigh scattering.

The optical depth of liquid water clouds is calculated using the parameterisation of Slingo (1989),

$$\tau_w = \mathrm{LWP}\left(a_i + \frac{b_i}{r_{eff}}\right). \quad (1)$$

Here LWP is the liquid water path of the cloud, a_i and b_i are parameters and r_{eff} is the effective radius of the water droplets. The parameters, which are taken to be $-8.9\,m^2\,kg^{-1}$ and $1.67 \times 10^3\,m\,kg^{-1}$, are updated from Edwards and Slingo (1996). The effective radius is assumed to be 6 µm over land and 12 µm over water.

The optical depth of ice water clouds is calculated using the non spherical parameterisation of Edwards et al. (2007),

$$\tau_i = \mathrm{IWP}\left(c_i + \frac{d_i}{d_{eff}} + \frac{e_i}{d_{eff}^2}\right). \quad (2)$$

Here IWP is the ice water path of the cloud, c_i, d_i and e_i are parameters updated to account for the different spectral bands and d_{eff} is the effective diameter of the ice particles. The values of c_i, d_i and e_i are $-2.189\,m^2\,kg^{-1}$, $3.311 \times 10^{-3}\,m\,kg^{-1}$ and $3.611 \times 10^{-12}\,kg^{-1}$, respectively. The effective diameter is taken to be 100 µm.

Neu et al. (2007) noted the importance of accounting for the effects of overlapping cloud layers, describing several means of doing it. We account for this effect using the simple approach of Briegleb (1992) where the optical depth is modified by the factor $f^{3/2}$, where f is the fraction of each grid box area covered by clouds. This has been demonstrated by Feng et al. (2004) to produce a computationally cheap representation of the effects of overlapping cloud layers being used extensively in global models (Liu et al., 2006; Voulgarakis et al., 2009).

GMDD
5, 3217–3260, 2012

The only aerosol accounted for at present is sulphate (Bellouin et al., 2007). The effect of hygroscopic growth on particle size and optical depth is parameterised using the approach of Fitzgerald (1975) as used by Bellouin et al. (2007).

All optical depths are determined at 600 nm and then scaled for the different wavelength bins. For the purposes of determining the addition of extra levels in the presence of high optical depths, only the cloud optical depth is used.

3.2 Calculation of cross sections

The cross sections are based on v6.4 of the file available from the Fast-JX website (Prather et al., 2010). This data set is a combination from the JPL14 assessment (Sander et al., 2003) with the addition of IUPAC data for NO_2 and VOC photolysis frequencies and of other sundry additions such as the acetone photolysis of Blitz et al. (2004) and the infrared photolysis of HO_2NO_2 of Jiménez et al. (2005). We have updated these frequencies to include data from JPL15 assessment (Sander et al., 2006), with the most notable changes including updates for N_2O_5 and OClO photolysis. We summarise all reactions described, noting whether they are utilised by the stratospheric or tropospheric chemistry, in Table A1.

4 Methodology

To test the performance of the model we carry out a series of tests. The first of these is to investigate how the photolysis code performs under idealised conditions. To do this we employ the scenarios devised for the PHOTOCOMP photolysis study as part of the CCMVal chemistry climate model intercomparison (Chipperfield et al., 2010).

We then proceed to investigate how the MetUM model with the Fast-JX photolysis included performs. To do this we perform a run with the tropospheric chemistry version of the model, from 2004 to 2008 and compare to different sets of observations including data from the INTEX campaign and the TES satellite. To enable us to make more

GMDD
5, 3217–3260, 2012

direct comparisons we run the model in "nudged mode" (Telford et al., 2008). This constrains the model to meteorological observations making comparisons with data over our chosen years more meaningful.

The first brief check we make is to ensure that nudging with the ERA-Interim dataset is as successful as nudging with the ERA-40 dataset. We do this by comparing biases, correlations and root mean squared differences between the nudged model and analyses as used by Telford et al. (2008). We then proceed to compare photolysis frequencies with observations from the INTEX-NA campaign, sampling the model at the time and location of the measurements. We make a quantitative assessment of the climatological and interactive photolysis schemes by comparing biases, correlations and root mean squared differences (RMSD) between the model and the observations.

We then study the effects these changes in photolysis frequencies have on atmospheric composition, focusing on ozone and carbon monoxide. Our principal comparisons are with observations from the TES satellite, comparing both the distributions of CO and O_3 and their correlation. We sample the model in a similar manner to Rodgers and Connor (2003), taking measurements at the appropriate time and location as the satellite and applying the instrument's averaging kernels to make comparisons more meaningful. To understand the changes in the chemical species distributions we also study the ozone budgets and changes in OH.

5 Model results

5.1 Idealised comparison

We first check the photolysis frequencies of NO, O_2 and O_3[3] under idealised conditions using the three assessed scenarios from the PHOTOCOMP assessment of the CCMVal model intercomparison (see Sect. 6.3.1 in Chipperfield et al., 2010). These employed idealised atmospheric conditions to allow systematic comparisons between

[3]This is the total O_3 photolysis frequency.

GMDD
5, 3217–3260, 2012

the photolysis in different models. The three scenarios used clear sky conditions with a solar zenith angle of 15°, 84° and averaged over a day between 84° and 96°.

First we compare photolysis frequencies as a function of altitude in a series of idealised atmospheric profiles constructed for a multi model comparison study. The photolysis frequencies for NO, O_2 and O_3 and Cl_2O_2 are shown in Fig. 1, which can be compared to Fig. 6.1 in Chipperfield et al. (2010).

The O_3 photolysis frequencies look similar to the PHOTOCOMP average, reducing from around $10^{-2}\,s^{-1}$ at 0.1 hPa to between 10^{-4}–$10^{-3}s^{-1}$near the surface, depending on the solar zenith angle. Similarly the O_2 photolysis frequencies look similar to the PHOTOCOMP average, reducing from around $10^{-9}s^{-1}$ at 0.1 hPa to below $10^{-14}\,s^{-1}$ between 20 and 200 hPa depending on the solar zenith angle. The NO photolysis frequencies are the exception, being high biased throughout the atmosphere. At the top of the atmosphere the photolysis frequencies are around $10^{-5}\,s^{-1}$ in contrast to the PHOTOCOMP average, which is nearer to $10^{-6}\,s^{-1}$. This is consistent with the models that employ Fast-JX in the PHOTOCOMP study, which see good agreement with the multi model mean photolysis frequencies for O_2 and O_3, but report a high bias in the case of NO. This discrepancy has been linked to factors such as a neglect of NO absorption in the calculation of the optical depth, leading to an overestimate of the modelled cross section.

Given the general successful performance under idealised conditions we move on to studying the effects of the photolysis code within the wider chemistry climate model.

5.2 Validation of nudged tropospheric MetUM run

After demonstrating that the photolysis schemes works well under idealised conditions we test the performance of the scheme within a MetUM model run.

GMDD
5, 3217–3260, 2012

5.2.1 Validation of nudging with ERA-Interim analyses

As this is the first time we have used ERA-Interim re-analysis data in the nudging we briefly re-evaluate the nudging performance. To do this we use the simple statistical tests of Telford et al. (2008), calculating the bias, correlation and root mean squared difference between the nudged model and the ERA-Interim data. These results are shown in Table 1. The performance of the nudging is broadly similar to that when using ERA-40 (compare to Table 1 in Telford et al., 2008), with the most notable difference being the reduction in the RMSE of potential temperature (θ), which probably reflects that improvements in the ERA-Interim analyses. From these results we conclude that the model nudged towards the ERA-Interim analyses can be used as a hindcast of the period 2004 to 2008. This is consistent with the results of Kipling et al. (2012) who show that nudging towards ERA-Interim analyses was able to improve modeled aerosol properties.

5.2.2 Comparison of cloud optical depth

The greatest values and variability in the tropospheric optical depth arise from clouds. To demonstrate the model is able to provide a reasonable description of this cloud optical depth we compare our modelled distribution with satellite data. Because of its high temporal resolution, we chose to compare to the ISCCP (International Satellite Cloud Climatology Project) D2 data-sets (Rossow et al., 1996; Rossow and Schiffer, 1999), which are constructed from the output of several NOAA (the American National Oceanic Atmospheric Administration) satellites. The comparisons for December, January and February 2005 and June to August 2005 are shown in Fig. 2.

The model is able to capture many of the features of the observations. For instance the storm tracks in the Northern Atlantic and Pacific oceans are well reproduced as are the decks of stratus clouds off the coast of Peru. There are some discrepancies between the model and data, for instance the model underestimates the optical depth in the inter tropical convergence zone (ITCZ). Some of the other differences can be

GMDD
5, 3217–3260, 2012

attributed to issues with the data, with errors introduced at high solar zenith angles, contamination from dust and an underestimate of the amount of optically thick cloud (Marchand et al., 2010). For instance the discrepancy between the model and observations over the Sahara is a result of factors such as dust in the measurements rather than a deficiency in clouds in the model. However some of the discrepancies can be attributed to the simplified calculation of cloud optical depth and the limited resolution of the model. From the general good agreement we conclude that the model is able to provide a reasonable description of the cloud optical depth, with the agreement being at least as good as that in other models (see e.g. Voulgarakis et al., 2009).

5.2.3 Comparison of photolysis frequencies with INTEX campaign data

Although the modelled photolysis performs well under an idealised scenario, to more fully evaluate its performance we compare the modelled photolysis frequencies, with the interactive and climatological photolysis schemes, to observational data. The observations we choose to use are from the INTEX-A flight campaign, conducted over North America and the Atlantic in the summer of 2004 (Singh et al., 2006). On these flights the actinic flux was measured in different wavelength regions using spectral radiometers and photolysis frequencies are obtained by multiplying by cross sections from Sander et al. (2003). This procedure to measure photolysis frequencies has been reported to be accurate to around 15–20 % (Shetter and Müller, 1999).

The use of the nudged version of the MetUM model allows us to make meaningful comparisons with the campaign data on a measurement by measurement basis. To do this we sample the model at the same time and location as the measurements were made, an approach similar to O'Connor et al. (2005) and employed by Kipling et al. (2012), interpolating the model to the pressure and co-ordinates where the measurements were made. As noted by O'Connor et al. (2005), the relatively low resolution that we use will prevent us from resolving small scale features in the observations. However we expect that we can produce the larger scale features relating to altitude, latitude and time of day. Figure 3 shows the O_3 and NO_2 photolysis frequencies from the first flight

GMDD
5, 3217–3260, 2012

of the INTEX-NA campaign (1 July 2004) and in the MetUM model, with and without interactive photolysis frequencies.

The O_3 photolysis rate is shown to be significantly improved by the use of the interactive photolysis frequencies, with the low bias removed. The capture of the variability of the photolysis frequencies is also improved, reflecting the improved ability of the interactive photolysis frequencies to model the effects of variations in optical depth. The improvement in the NO_2 photolysis rate is not as dramatic, though it can be seen that the interactive photolysis reduces a smaller bias and captures the variability better.

Figure 3 only shows one flight from the entire campaign. Although we chose this at random, selecting the first flight in the data, it is possible that the conditions might favour one photolysis scheme in particular. Therefore we calculate the bias, correlation and, root mean squared difference (RMSD) between the modelled photolysis frequencies and the observed frequencies for all flights. The biases provide information on average frequencies. The correlations indicate the ability of the model to capture the variability in the photolysis. The RMSD combines information about average agreement and variability. The biases, correlations and RMSD are given in Table 2 for the two frequencies shown in Fig. 3, along with selected other frequencies.

The tabulated results are in accord with Fig. 3, with the interactive photolysis having lower biases and higher correlations with the data than the climatological photolysis. For several reactions, including O_3 photolysis, the discrepancy between the climatological photolysis and the data is considerably larger than the reported experimental uncertainty. For the interactive photolysis there are much smaller differences between the average model and observed values. Some of the reactions where there are differences between the model and the interactive photolysis and data, most notably HONO, are those where there have been updates to the reference cross sections. In the case of HONO the values (Sander et al., 2006) used in the interactive photolysis now incorporate additional measurements (Kenner and Stuhl, 1986; Stutz et al., 2000). This is relevant as the observed photolysis frequencies are not measured directly, but are a product of the measured radiation multiplied by cross sections from Sander et al.

GMDD
5, 3217–3260, 2012

(2003). So some of the discrepancy can be attributed to an improved understanding of the experimental cross sections. Whilst some of the bias with the climatological scheme can be attributed to the use of old photolysis frequency measurements and a simple treatment of cloud optical depth, much can be attributed to an overestimation of the stratospheric ozone column.

By inspecting Fig. 3 we also see, as expected, that the global model, with either photolysis scheme, is not designed to describe small scale variations. However the use of the interactive photolysis, rather than the climatological scheme does produce notable improvements. The correlation between the interactive photolysis and data is always greater than 0.8 and only greater than 0.8 for the photolysis frequencies of one species, HCHO, with the climatological scheme. This is as expected as the photolysis frequencies are now sensitive to changes in cloud optical depth.

Although the Fast-JX code is designed to run using 18 wavelength bins it can be run using a subset of 8 or 12 of these, where the lower wavelength bins are excluded. We repeated the comparison between the model with the default Fast-JX model and with 8 and 12 bins. The largest differences are found in the ozone photolysis frequencies. The photolysis frequencies with 8 and 12 bins only differ slightly from each other, but at high altitudes are appreciably lower than the default scheme. The difference can be as large as 7 % with an average bias of 1 %. The correlation and RMSE are unchanged to two significant figures. However for studies focussed on the lower troposphere the reduced wavelength bin schemes are acceptable, though for studies that examine the upper troposphere and stratosphere the default setting, that of using all 18 wavelength bins, would be required.

5.2.4 Comparison of ozone and carbon monoxide to TES measurements

After demonstrating that the photolysis frequencies look reasonable we investigate their effects on the tracer distributions, comparing model simulations, with the climatological and interactive photolysis schemes, and measurements. The large spatial and

GMDD
5, 3217–3260, 2012

temporal scales of satellite observations make them ideal to be employed in this capacity. We compare to observations of ozone and carbon monoxide from the TES satellite.

The Tropospheric Emission Spectrometer (TES) is an infrared Fourier transform spectrometer (Beer et al., 2001) onboard NASA's Aura satellite which was launched in 2004. In this study we utilise CO and ozone profile observations from the TES Global Survey mode. In this mode profiles have a nadir footprint of 5.3 × 8.3 km and are spaced approximately 180 km apart along the orbital track with a 16 day repeat cycle.

In order to be able to make systematic comparisons between the model and the TES observations we have developed code that samples the model online at the times and locations of the satellite measurements. This differs slightly from the technique used in previous studies, such as those by Voulgarakis et al. (2011), who took relatively high frequency global (six hourly) averages and sampled these as close to the time and location of the TES measurements as possible. After interpolating the modelled values of O_3 and CO onto pressure levels used by the TES retrievals, we here we apply averaging kernels following the method of Rodgers and Connor (2003), a procedure which is shown to be vital by the study of Aghedo et al. (2011). We bin the O_3 and CO data from the model and the data into $4^\circ \times 5^\circ$ bins and average from 800–400 hPa.

First we compare the ozone distributions between the model, with interactive and climatological photolysis schemes, and the TES observations (Nassar et al., 2008) (Fig. 4). For consistency with Voulgarakis et al. (2011) we compare for the periods July to August and January to February. With either photolysis schemes the model captures the main features such as the low ozone values over the Western tropical Pacific and the products of biomass burning from Southern Africa. The modelled ozone, with either photolysis schemes, is slightly higher (9 % averaged over both periods) than the observations. Validation of TES ozone profiles against ozonesondes and LIDAR observations have shown that TES itself has a mean high bias in this altitude region of 5–10 % (Nassar et al., 2008; Richards et al., 2008). This contrasts to the previous version of the model which had a slight low bias (see Fig. 2 in Voulgarakis et al., 2011) . This increase is believed to mainly arise from changes in the underlying climate model.

GMDD
5, 3217–3260, 2012

To probe why the changes in photolysis have such a slight impact on the ozone we tabulate the budget of ozone in Table 3, where we compare the chemical production and loss of ozone, its source from the stratosphere (STE) and its sink to the surface by deposition. We also include the total ozone burden and methane lifetime. As well as the budget from the model with climatological and interactive photolysis we include a multi model average from Stevenson et al. (2006) and results from another version of the MetUM model that employs the interactive photolysis, albeit with simpler tropospheric chemistry (Morgenstern et al., 2012).

We can see that the change in photolysis scheme has a large effect on the chemical production and loss terms, but that the overall, global, effect is small as the changes balance each other. The interactive photolysis has production and loss terms more similar to the multi model average of Stevenson et al. (2006). The model of Morgenstern et al. (2012) has smaller chemical fluxes which can be accounted for by its simpler tropospheric chemistry. However, whilst using the same implementation of the interactive photolysis scheme, it produces a relatively low ozone burden and high methane lifetime, indicating that the low methane lifetime seen in the tropospheric chemistry scheme in Table 3 is not solely a result of the interactive photolysis.

Next we compare the carbon monoxide distributions between the model, with interactive and climatological photolysis schemes, and the TES observations (Luo et al., 2007; Lopez et al., 2008) (Fig. 5). Again we compare for the periods July to August and January to February.

The differences between the two versions of the model are now more dramatic. Again both versions capture the broad features with high values of carbon monoxide produced by biomass burning, in particular from Africa, and anthropogenic emissions from Asia. However whilst the model with climatological photolysis has only a small bias (2 %), when the interactive photolysis is employed there is a large negative bias (−24 %). Although there are small positive biases (less than 10 %) in the tropics and small negative biases in midlatitudes (less than 10 %) in the observations (Luo et al., 2007; Lopez et al., 2008), this model bias is significant. As the emissions

GMDD
5, 3217–3260, 2012

are unchanged between the two models then we ascribe these changes to the main sink of CO, its reaction with the hydroxyl radical, OH. Indeed if we look at the methane lifetime (Table 3), which is dominated by its reaction with OH, we see that this is greatly reduced by switching from the climatological to interactive photolysis scheme. We can look directly at the changes in the OH by plotting the OH field, weighted as in Lawrence et al. (2001), with the climatological and interactive photolysis schemes (Fig. 6).

We first note that the use of the interactive photolysis scheme increases the total OH burden, which explains the decreased CO concentrations and CH_4 lifetimes. We also note that the amount of OH is now significantly higher than that reported by Spivakovsky et al. (2000) leading us to believe that the amount of OH is excessive. To understand the increase we examined the production and loss terms of HO_x ($\equiv OH+HO_2$) and found that the increases in HO_x are dominated by increases in its production via $O(^1D)+H_2O$. The water vapour is constant between the two simulations and in a recent study found to compare reasonably well with other models and observations (Russo et al., 2011). Therefore the increase must arise from increased production of $O(^1D)$, which is produced from the photolysis of ozone. This is greatly increased by using the interactive scheme as can be seen from Fig. 3. However we believe that the increased $j(O(^1D))$ is realistic.

The apparently superior performance of the climatological photolysis scheme is a result of two conflicting factors, the high bias in ozone and the low bias in the ozone photolysis frequencies. Removing one of these factors, although an improvement in itself, thus worsens the performance of some aspects of the model. Indeed Morgenstern et al. (2012) see no such problems with high biases in OH despite using this implementation of the interactive photolysis scheme, albeit with a considerably different chemistry scheme. Results from a more complete whole atmospheric chemistry (Archibald et al., 2012) also indicate lower ozone concentrations produce lower OH concentrations, higher CO concentrations and a longer methane lifetime.

Finally, adopting the approach of Voulgarakis et al. (2011), we compare the O_3–CO correlations using them to understand the models performance (Fig. 7). Like previous

GMDD
5, 3217–3260, 2012

versions of the model (Voulgarakis et al., 2011) the O_3–CO correlation is lower in the MetUM model than in the observations. This may reflect the use of climatological biomass burning emissions, which would tend to reduce correlations. On a global scale the two versions of the model perform similarly with "scores" of 0.3 for both photolysis schemes for both periods. The "scores" are obtained by correlating the tracer-tracer correlations in the model and observations. However there are different regions where the two photolysis schemes perform better, with the interactive photolysis producing better agreement near sources of biomass burning (S. America; Central Africa) and the climatological scheme performing more strongly in the extra-tropics. This worsening of performance of the interactive photolysis scheme can be linked to the high OH concentrations attenuating CO concentrations too rapidly with distance from sources.

5.2.5 Conclusions with regards to tropospheric run

We have evaluated the performance of the Fast-JX photolysis scheme in the tropospheric version of the MetUM model using a nudged run between 2004 and 2008. After briefly checking that nudging to the ERA-Interim analyses is successful, and that the modelled cloud optical depths were realistic, we proceeded to demonstrate improvements to the modelled photolysis frequencies using comparisons to data from the INTEX-NA campaign. These results showed that the online photolysis model provides a significantly better description of the observed frequencies. We then investigated the effects that these improved photolysis frequencies have on the modelled chemical fields, comparing the changes to observations from the TES satellite. The improved photolysis frequencies, whilst producing some improvements to the chemical fields, produced a high bias in the global burden of OH, which itself affected CO concentrations and the CH_4 lifetime. This was as a result of the more realistic photolysis frequencies increasing the sensitivity of the model to high biases in ozone, the effects of which in the climatological photolysis scheme were masked by too small ozone photolysis frequencies.

GMDD
5, 3217–3260, 2012

5.3 Stratospheric chemistry

In addition to testing the model in the troposphere a further simple validation was performed in the stratosphere. In order to test the feedback from chemical changes onto the dynamics we ran the model unconstrained by nudging. The run we perform is similar to that used in Morgenstern et al. (2009), which itself follows the definition of the REF-B0 experiment of the CCMVal model intercomparison (Eyring et al., 2010). This uses forcings that represent perpetual 2000 conditions, although, as we are able to initialise the chemical fields from those in Morgenstern et al. (2009) we only perform a 10 yr run, discarding the first five years as "spin-up".

In Fig. 8 we examine the average annual cycle of the total ozone column. The values from the model are compared to a combination of data from a variety of sources including TOMS, SBUV, GOME and OMI, for the year 2000 (Bodeker et al., 2005). The model captures most of the features including the latitudinal gradient and timing and magnitude of the Northern Hemisphere spring maximum.

The previous version of the chemistry scheme had some discrepancies with observations around the tropopause, including high biases in temperature and ozone (Morgenstern et al., 2009). To assess how the updated model performs we compare ozone profiles with those from the SHADOZ network (Thompson et al., 2003a,b). We show results from one representative site, Fiji, in Fig. 9 displaying monthly mean ozone profiles as a function of pressure. The model is able to capture the seasonal cycle well, though it does still slightly overestimate UTLS ozone. Tropospheric ozone is slightly low, as should be expected, as this version of the model does not attempt to fully simulate tropospheric emissions and chemistry.

6 Discussion

Whilst we have demonstrated that the photolysis frequencies are improved by the use of the interactive photolysis scheme and that the stratospheric version of the model

GMDD
5, 3217–3260, 2012

performs well with it there are still obvious issues with the tropospheric model. We have demonstrated that these arise from high biases in the ozone concentrations which, without the large low bias in photolysis frequencies seen in the climatological scheme, now produce a high bias in OH.

We have reduced the O_3 high bias by various measures, including the replacement of the original upper boundary condition for NO_y as used by O'Connor et al. (2009) with one from the Cambridge-2D model, adding of the reaction between HO_2 and NO using the rates and yields of Butkovskaya et al. (2007) and adding the hydrolysis of N_2O_5 (Morgenstern et al., 2009). Whilst these reduced the biases in ozone they did not eliminate them. Further work is being carried out at present to try and understand the sources of these biases, but they cannot obscure the improved description of observed photolysis rates by the interactive photolysis scheme as opposed to the climatological scheme.

Even with the resolution of the issues with biases in ozone there are still a potential ways of expanding the capability of the interactive photolysis scheme. One obvious omissions regards the limited use of aerosols in the model. This will change when the GLOMAP-mode scheme (Mann et al., 2010) is coupled to the photolysis. Although on a global scale aerosols are less important than clouds for the optical depth calculation there are specific episodes where this coupling will be useful. A further improvement, of more import for the stratosphere, will be the use of a variable solar constant, a driver of some of the variability in stratospheric ozone. Whilst our simple approach of accounting for overlapping cloud layers seems to work at present, increasing vertical resolution may require more sophisticated techniques to be employed (Neu et al., 2007). The new techniques we describe for validating the model will also be useful in assessing other aspects of the model performance.

GMDD
5, 3217–3260, 2012

7 Conclusions

We describe the implementation of the Fast-JX interactive photolysis scheme in the UK Met Office Unified Model. The interactive photolysis scheme is shown to improve the modelled photolysis frequencies from the previous, climatological scheme in comparison to observations and other models. The effect on atmospheric composition is less clear cut, with the interactive photolysis scheme producing too much OH. However this is believed to be a result of a previous cancellation of errors being removed, and not as a result of any inherent problem with the interactive photolysis scheme. As well as being a more realistic manner of modelling the photolysis the interactive photolysis will permit more detailed studies of the interactions between the atmosphere and its constituents.

Acknowledgements. We acknowledge NCAS and NCEO for their funding of this work. MD and FMOC were supported by the Joint DECC/Defra Met Office Hadley Centre Climate Programme (GA01101).

We thank Michael Prather for the provision of the Fast-JX code and Oliver Wild and Apostolos Voulgarakis for insights into its operation. We thank Martyn Chipperfield for his help in comparing to the PHOTOCOMP model intercomparison. We thank Glenn Carver and Nick Savage for discussions about the flight track sampling code. We thank Maria Russo for discussions about water vapour and clouds. We acknowledge James Keeble for his work in assisting understanding of the updated stratospheric chemistry.

Biogenic emissions were obtained from the GEIA centre http://www.geiacenter.org/inventories/present.html. The INTEX-NA data was obtained from the NASA-LARC website http://www-air.larc.nasa.giv/missions/intexna/intexna.htm. The ISCCP D2 data/images were obtained from the International Satellite Cloud Climatology Project web site http://isccp.giss.nasa.gov maintained by the ISCCP research group at the NASA Goddard Institute for Space Studies, New York, NY. on March, 2010 (Rossow and Schiffer, 1999). We would like to thank Greg Bodeker of Bodeker Scientific for providing the combined total column ozone database (http://www.bodekerscientific.com/data/total-column-ozone). We thank the NASA Langley Research Center Atmospheric Science Data Center for the TES data.

GMDD

5, 3217–3260, 2012

References

Aghedo, A. M., Bowman, K. W., Shindell, D. T., and Faluvegi, G.: The impact of orbital sampling, monthly averaging and vertical resolution on climate chemistry model evaluation with satellite observations, Atmos. Chem. Phys., 11, 6493–6514, doi:10.5194/acp-11-6493-2011, 2011. 3232

Archibald, A. T., Abraham, N. L., Braesicke, P., Dalvi, M., Johnson, C., Keeble, J. M., O'Connor, F. M., Squire, O. J., Telford, P. J., and Pyle, J. A.: Evaluation of the UM-UKCA model configuration for Chemistry of the Stratosphere and Troposphere (CheST), Geosci. Model Dev., in preparation, 2012. 3218, 3234

Beer, R., Glavic, T., and Rider, M.: Tropospheric emission spectrometer for the Earth observing System's Aura Satellite, Appl. Optics, 40, 2356–2367, 2001. 3232

Bellouin, N., Boucher, O., Haywood, J., Johnson, C., Jones, A., Rae, J., and Woodward, S.: Improved representation of aerosols for HadGEM2, Tech. rep., Met Office Hadley Centre, 2007. 3225

Bian, H. and Prather, M.: Fast-J2: accurate simulation of stratopheric photolysis in global chemical models, J. Atmos. Chem., 41, 281–296, 2002. 3222

Blitz, M., Heard, D., and Pilling, M.: Pressure and temperature-dependent quantum yields for the photodissociation of acetone between 279 and 327.5 nm, Geophys. Res. Lett., 31, L06111, doi:10.1029/2003GL018793, 2004. 3225, 3250

Bodeker, G. E., Shiona, H., and Eskes, H.: Indicators of Antarctic ozone depletion, Atmos. Chem. Phys., 5, 2603–2615, doi:10.5194/acp-5-2603-2005, 2005. 3236, 3259

Briegleb, P.: Delta-eddington approximation for solar radiation in the ncar community climate models, J. Geophys. Res., 97, 7603–7612, 1992. 3224

Butkovskaya, N. I., Kukui, A., and Le Bras, G.: HNO_3 forming channel of the $HO_2 + NO$ reaction as a function of pressure and temperature in the ranges of 72–600 Torr and 223–323 K, J. Phys. Chem. A, 111, 9047–9053, 2007. 3220, 3237

Chipperfield, M., Kinnison, D., Bekki, S., Bian, H., Brühl, C., Canty, T., Cionni, I., Dhomse, S., Froidevaux, L., Fuller, R., Müller, R., Prather, M., Salawitch, R., Santee, M., Tian, W., and Tilmes, S.: SPARC CCMVal Report on the Evaluation of Chemistry-Climate Models, Stratospheric Chemistry, chapter 6, 191–252, SPARC, http://homepages.see.leeds.ac.uk/~lecmc/ccmvalj/, 2010. 3219, 3225, 3226, 3227, 3252

GMDD
5, 3217–3260, 2012

Dall'Amico, M., Gray, L., Rosenlof, K., Scaife, A., Shine, K., and Stott, P.: Stratospheric temperature trends: impact of ozone variability and the QBO, Clim. Dynam., 34, 381–398, doi:10.1007/s00382-009-0604-x, 2010. 3220

Dee, D., Uppala, S., Simmons, A., Berrisford, P., Poli, P., Kobayashi, S., Andrae, U., Balmaseda, M. A., Balsamo, G., Bauer, P., Bechtold, P., Beljaars, A. C. M., van de Berg, L., Bidlot, J., Bormann, N., Delsol, C., Dragani, R., Fuentes, M., Geer, A. J., Haimberger, L., Healy, S. B., Hersbach, H., Hólm, E. V., Isaksen, L., Kållberg, P., Köhler, M., Matricardi, M., McNally, A. P., Monge-Sanz, B. M., Morcrette, J.-J., Park, B.-K., Peubey, C., de Rosnay, P., Tavolato, C., Thépaut, J.-N., and Vitart, F.: The ERA-Interim reanaysis: configurationa and performance of the data analysis system, Q. J. Roy. Meteor. Soc., 137, 553–597, doi:10.1002/qj.828, 2011. 3220

Edwards, J. and Slingo, A.: Studies with a flexible new radiation code. I: Choosing a configuration for a large-scale model, Q. J. Roy. Meteor. Soc., 122, 689–719, 1996. 3224

Edwards, J. M., Havemann, S., Thelen, J.-C., and Baran, A.: A new parameterisation for the radiative properties of ice crystals, comparison of existing schemes and impact in a GCM, Atmos. Res., 83, 19–35, doi:10.1016/j.atmosres.2006.03.002, 2007. 3224

Eyers, C., Addleton, D., Atkinson, K., Broomhead, M., Christou, R., Elliff, T., Falk, R., Gee, I., Lee, D., Marizy, C., Michot, S., Middel, J., Newton, P., Norman, P., Plohr, M., Raper, D., and Stanciou, N.: AERO2K global aviation emissions inventories for 2002 and 2025, Tech. Rep. 04/01113, Qinetiq, http://aero-net.info/fileadmin/aeronet_files/links/documents/AERO2K_Global_Aviation_Emissions_Inventories_for_2002_and_2025.pdf, 2004. 3220

Eyring, V., Shepherd, T., and Waugh, D.: SPARC Report on the Evaluation of Chemistry-Climate Models, Tech. rep., SPARC Report No. 5, WCRP-132, WMO/TD-N0. 1526, http://www.atmosp.physics.utoronto.ca/SPARC/ccmval_final/index.php, 2010. 3236

Feng, Y., Penner, J. E., Sillman, S., and Liu, X.: Effects of cloud overlap in photochemical models, J. Geophys. Res., 109, D04310, doi:10.1029/2003JD004040, 2004. 3224

Fitzgerald, J.: Approximation formulas for the equilibrium size of an aerosol particle as a function of its dry size and composition and the ambient relative humidity, J. Appl. Meteorol., 14, 1044–1049, doi:10.1175/1520-0450(1975)014<1044:AFFTES>2.0.CO;2, 1975. 3225

Giannakopoulos, C., Chipperfield, M., Law, K., and Pyle, J.: Validation and intercomparison of wet and dry deposition schemes using Pb-210 in a global three-dimensional off-line chemical transport model, J. Geophys. Res., 104, 23761–23784, 1999. 3220

GMDD
5, 3217–3260, 2012

Guenther, A., Hewitt, C. N., Erickson, D., Fall, R., Geron, C., Graedel, T., Harley, P., Klinger, L., Lerdau, M., McKay, W. A., Pierce, T., Scoles, B., Steinbrecher, R., Tallaamraju, R., Taylor, J., and Zimmerman, P.: A global model of natural volatile organic compound emissions, J. Geophys. Res., 100, 8873–8892, 1995. 3220

Hewitt, H. T., Copsey, D., Culverwell, I. D., Harris, C. M., Hill, R. S. R., Keen, A. B., McLaren, A. J., and Hunke, E. C.: Design and implementation of the infrastructure of HadGEM3: the next-generation Met Office climate modelling system, Geosci. Model Dev., 4, 223–253, doi:10.5194/gmd-4-223-2011, 2011. 3219

Hough, A. M.: The calculation of photolysis rates for use in global modelling studies, Tech. rep., UK Atomic Energy Authority, Harwell, Oxon., UK, 1988. 3222

Jiménez, E., Gierczak, T., Stark, H., Burkholder, J. B., and Ravishankara, A. R.: Quantum yields of OH, HO_2 and NO_3 in the UV photolysis of HO_2NO_2, Phys. Chem. Chem. Phys., 7, 342–348, 2005. 3225, 3250

Kenner, R. D., Rohrer. F., and Stuhl, F.: Hydroxyl (A) production in the 193-nm photolysis of nitrous acid, J. Phys. Chem., 90, 2635–2639, 1986. 3230

Kipling, Z., Stier, P., Schwarz, J. P., Fahey, D. W., Spackman, J. R., Mann, G. W., Johnson, C. E., and Telford, P. J.: Constraints from vertically-resolved aircraft observations on aerosol processes in climate models, Atmos. Chem. Phys., in preparation, 2012. 3228, 3229

Lamarque, J.-F., Bond, T. C., Eyring, V., Granier, C., Heil, A., Klimont, Z., Lee, D., Liousse, C., Mieville, A., Owen, B., Schultz, M. G., Shindell, D., Smith, S. J., Stehfest, E., Van Aardenne, J., Cooper, O. R., Kainuma, M., Mahowald, N., McConnell, J. R., Naik, V., Riahi, K., and van Vuuren, D. P.: Historical (1850–2000) gridded anthropogenic and biomass burning emissions of reactive gases and aerosols: methodology and application, Atmos. Chem. Phys., 10, 7017–7039, doi:10.5194/acp-10-7017-2010, 2010. 3220

Lamarque, J.-F., Emmons, L. K., Hess, P. G., Kinnison, D. E., Tilmes, S., Vitt, F., Heald, C. L., Holland, E. A., Lauritzen, P. H., Neu, J., Orlando, J. J., Rasch, P. J., and Tyndall, G. K.: CAM-chem: description and evaluation of interactive atmospheric chemistry in the Community Earth System Model, Geosci. Model Dev., 5, 369–411, doi:10.5194/gmd-5-369-2012, 2012. 3257

Lary, D. and Pyle, J.: Diffuse-radiation, twilight, and photochemistry, J. Atmos. Chem., 13, 393–406, 1991. 3222, 3223

Law, K. and Pyle, J.: Modeling trace gas budgets in the troposphere 1. ozone and odd nitrogen, J. Geophys. Res., 98, 18377–18400, 1993a. 3220

GMDD
5, 3217–3260, 2012

Law, K. and Pyle, J.: Modeling trace gas budgets in the troposphere 2. CH_4 and CO, J. Geophys. Res., 98, 18401–18412, 1993b. 3220

Law, K., Plantevin, P., Shallcross, D., Rogers, H., Pyle, J., Grouhel, C., Thouret, V., and Marenco, A.: Evaluation of modeled O_3 using Measurement of Ozone by Airbus In-Service Aircraft (MOZAIC) data, J. Geophys. Res., 103, 25721–25737, 1998. 3222

Lawrence, M. G., Jöckel, P., and von Kuhlmann, R.: What does the global mean OH concentration tell us?, Atmos. Chem. Phys., 1, 37–49, doi:10.5194/acp-1-37-2001, 2001. 3234, 3257

Liu, H., Crawford, J., Pierce, R., Norris, P., Platnick, S., Chen, G., Logan, J., Yantosca, R., Evans, M., Kittaka, C., Feng, Y., and Tie, X.: Radiative eddect of clouds on tropspheric chemistry in a global three-dimensional chemical transport model, J. Geophys. Res., 111, D20303, doi:10.1029/2005JD006403, 2006. 3218, 3224

Lopez, J. P., Luo, M., Christensen, L. E., Loewenstein, M., Jost, H., Webster, C. R., and Osterman, G.: TES carbon monoxide validation during two AVE campaigns using the Argus and ALIAS instruments on NASA's WB-57F, J. Geophys. Res., 113, D16847, doi:10.1029/2007JD008811, 2008. 3233

Luo, M., Rinsland, C., Fisher, B., Sachse, G., Diskin, G., Logan, J., Worden, H., Kulawik, S., Osterman, G., Eldering, A., Herman, R., and Shephard, M.: TES carbon monoxide validation with DACOM aircraft measurements during INTEX-B, J. Geophys. Res., 112, D24848, doi:10.1029/2007JD008803, 2007. 3233

Mann, G. W., Carslaw, K. S., Spracklen, D. V., Ridley, D. A., Manktelow, P. T., Chipperfield, M. P., Pickering, S. J., and Johnson, C. E.: Description and evaluation of GLOMAP-mode: a modal global aerosol microphysics model for the UKCA composition-climate model, Geosci. Model Dev., 3, 519–551, doi:10.5194/gmd-3-519-2010, 2010. 3218, 3237

Marchand, R., Ackerman, T., Smyth, M., and Rossow, W. B.: A review of cloud top height and optical depth histograms from MISR, ISCCP, and MODIS, J. Geophys. Res., 115, D16206, doi:10.1029/2009JD013422, 2010. 3229

Morgenstern, O., Braesicke, P., O'Connor, F. M., Bushell, A. C., Johnson, C. E., Osprey, S. M., and Pyle, J. A.: Evaluation of the new UKCA climate-composition model – Part 1: The stratosphere, Geosci. Model Dev., 2, 43–57, doi:10.5194/gmd-2-43-2009, 2009. 3218, 3220, 3221, 3222, 3236, 3237

Morgenstern, O., Zeng, G., Abraham, N., Telford, P., Braesicke, P., Pyle, J., Hardiman, S. C., O' Connor, F. M., and Johnson, C. E.: Impacts of climate change, ozone recovery, and increas-

GMDD
5, 3217–3260, 2012

ing methane on the tropospheric oxodising capacity, J. Geophys. Res., submitted, 2012. 3219, 3233, 3234, 3249

Nassar, R., Logan, J. A., Worden, H. M., Megretskaia, I. A., Bowman, K. W., Osterman, G. B., Thompson, A. M., Tarasick, D. W., Austin, S., Claude, H., Manvendra, K., Dubey, W., Hocking, K., Johnson, B. J., Joseph, E., Merrill, J., Morris, G. A., Newchurch, M., Oltmans, S. J., Posny, F., Schmidlin, F. J., Vömel, H., Whiteman, D. N., and Witte, J. C.: Validation of Tropospheric Emission Spectrometer (TES) nadir ozone profiles using ozonesonde measurements, J. Geophys. Res., 113, D15S17, 13 pp., doi:10.1029/2007JD008819, 2008. 3232

Neu, J., Prather, M., and Penner, J.: Global atmospheric chemistry: integrating over fractional cloud cover, J. Geophys. Res., 112, D11306, 12 pp., doi:10.1029/2006JD008007, 2007. 3222, 3224, 3237

O'Connor, F., Carver, G., Savage, N., Pyle, J. A., Methven, J., Arnold, S. R., Dewey, K., and Kent, J.: Comparison and visualisation of high resolution transport modelling with aircraft measurements, Atmos. Sci. Lett., 6, 164–170, doi:10.1002/asl.111, 2005. 3229

O'Connor, F., Johnson, C., Morgenstern, O., and Collins, W. J.: Interactions between tropospheric chemistry and climate model temperature and humidity biases, Geophys. Res. Lett, 36, L16801, doi:10.1029/2009GL039152, 2009. 3218, 3237

Parkinson, W., Rufus, J., and Yoshino, K.: Absolute absorption cross section measurements of CO_2 in the wavelength region 163–200 nm and the temperature dependence, Chem. Phys., 290, 251–256, 2003. 3250

Pöschl, U., von Kuhlmann, R., Poisson, N., and Crutzen, P.: Development and intercomparison of condensed isoprene oxidation mechanisms for global atmospheric modelling, J. Atmos. Chem., 37, 29–52, 2000. 3220

Price, C. and Rind, D.: Modelling global lightning distributions in a general circulation model, Mon. Weather Rev., 122, 1930–1939, 1994. 3221

Rayner, A., Rayner, N., Parker, D., Horton, E., Folland, C., Alexander, L., Rowell, D., Kent, E., and Kaplan, A.: Global analyses of sea surface temperature, sea ice, and night marine air temperature since the late nineteenth century, J. Geophys. Res., 108, 4407, 29 pp., doi:10.1029/2002JD002670, 2003. 3219

Richards, N. A. D., Osterman, G. B., Browell, E. V., Hair, J. W., Avery, M., and Li, Q.: Validation of Tropospheric Emission Spectrometer ozone profiles with aircraft observations during the intercontinental chemical transport experiment-B, J. Geophys. Res.-Atmos., 113, D16S29, doi:10.1029/2007jd008815, 2008. 3232

GMDD

5, 3217–3260, 2012

Rodgers, C. D. and Connor, B. J.: Intercomparison of remote sounding instruments, J. Geophys. Res.-Atmos., 108, 4116, doi:10.1029/2002jd002299, 2003. 3226, 3232

Rossow, W., Walker, A., Beuschel, D., and Roiter, M.: International Satellite Cloud Climatology Project (ISCCP) Documentation of New Cloud Datasets, Tech. rep., World Meteorological Organization, http://isccp.giss.nasa.gov/pub/documents/d-doc.pdf, 1996. 3228

Rossow, W. B. and Schiffer, R. A.: Advances in understanding clouds from ISCCP, B. Am. Meteorol. Soc., 80, 2261–2287, 1999. 3228, 3238

Russo, M. R., Marécal, V., Hoyle, C. R., Arteta, J., Chemel, C., Chipperfield, M. P., Dessens, O., Feng, W., Hosking, J. S., Telford, P. J., Wild, O., Yang, X., and Pyle, J. A.: Representation of tropical deep convection in atmospheric models – Part 1: Meteorology and comparison with satellite observations, Atmos. Chem. Phys., 11, 2765–2786, doi:10.5194/acp-11-2765-2011, 2011. 3234

Sander, S., Friedl, R., Golden, D., Kurylo, M. J., Huie, R., Orkin, V., Moortgat, G., Ravishankra, A., Kolb, C., Molina, M., and Finlayson-Pitts, B.: Chemical Kinetics and Photochemical Data for Use in Atmospheric Studies Evaluation Number 14, Tech. rep., JPL, http://jpldataeval.jpl.nasa.gov/pdf/JPL_02-25_rev02.pdf, 2003. 3225, 3229, 3230

Sander, S., Friedl, R., Golden, D. M., Kurylo, M., Moortgat, G., Keller-Rudek, H., Wine, P., Ravishankra, A. R., Kolb, C., Molina, M., Finlayson, B., Huie, R., and Orkin, V.: Chemical Kinetics and Photochemical Data for Use in Atmospheric Studies Evaluation Number 15, Tech. rep., NASA JPL, http://jpldataeval.jpl.nasa.gov/pdf/JPL_15_AllInOne.pdf, 2006. 3221, 3225, 3230, 3250, 3251

Shetter, R. E. and Müller, M.: Photolysis frequency measurements using actinic flux spectroradiometry during the PEM-Tropics mission: Instrumentation description and some result, J. Geophys. Res., 104, 5647–5661, 1999. 3229

Singh, H. B., Crawford, J. H., Jacob, D. J., and Russell, P. B.: Overview of the summer 2004 Intercontinental Chemical Transport Experiment–North America (INTEX-A), J. Geophys. Res., 111, D24S01, doi:10.1029/2006JD007905, 2006. 3229

Slingo, A.: A GCM parameterization for the shortwave radiative properties of water clouds, J. Atmos. Sci., 46, 1419–1427, 1989. 3224

Spivakovsky, C., Logan, J., Montzka, S., Balkanski, Y., Foreman-Fowler, M., Jones, D., Horowitz, L., Fusco, A., Brenninkmeijer, C., Prather, M., Wofsy, S., and McElroy, M.: Three-dimensional climatological distribution of tropospheric OH: update and evaluation, J. Geophys. Res., 105, 8931–8980, 2000. 3234, 3257

GMDD

5, 3217–3260, 2012

Stevenson, D., Dentener, F., Schultz, M., Ellingsen, K., van Noije, T., Wild, O., Zeng, G., Amann, M., Atherton, C., Bell, N., Bergmann, D., Bey, I., Butler, T., Cofala, J., Collins, W., Derwent, R., Doherty, R., Drevet, J., Eskes, H., Fiore, A., Gauss, M., Hauglustaine, D., Horowitz, L., Isaksen, I., Krol, M., Lamarque, J.-F., Lawrence, M., Montanaro, V., Iler, J.-F. M., Pitari, G., Prather, M., Pyle, J., Rast, S., Rodriguez, J., Sanderson, M., Savage, N., Shindell, D., Strahan, S., Sudo, K., and Szopa, S.: Multimodel ensemble simulations of present-day and near-future tropospheric ozone, J. Geophys. Res., 111, D08301, 23 pp., doi:10.1029/2005JD006338, 2006. 3233, 3249

Stutz, J., Kim, E. S., Platt, U., Bruno, P., Perrino, C., and Febo, A.: UV-visible absorption cross sections of nitrous acid, J. Geophys. Res., 105, 14585–14592, 2000. 3230

Telford, P. J., Braesicke, P., Morgenstern, O., and Pyle, J. A.: Technical Note: Description and assessment of a nudged version of the new dynamics Unified Model, Atmos. Chem. Phys., 8, 1701–1712, doi:10.5194/acp-8-1701-2008, 2008. 3219, 3226, 3228, 3247

Telford, P. J., Lathière, J., Abraham, N. L., Archibald, A. T., Braesicke, P., Johnson, C. E., Morgenstern, O., O'Connor, F. M., Pike, R. C., Wild, O., Young, P. J., Beerling, D. J., Hewitt, C. N., and Pyle, J.: Effects of climate-induced changes in isoprene emissions after the eruption of Mount Pinatubo, Atmos. Chem. Phys., 10, 7117–7125, doi:10.5194/acp-10-7117-2010, 2010. 3218, 3220

Thompson, A., Witte, J., McPeters, R., Oltmans, S., Schmidlin, F., Logan, J., M.Fujiwara, Kirchhoff, V., Posny, F., Coetzee, G., Hoegger, B., Kawakami, S., Ogawa, T., Johnson, B., Vömel, H., and Labow, G.: Southern Hemisphere Additional Ozonesondes (SHADOZ) 1998–2000 tropical ozone climatology 1. Comparison with Total Ozone Mapping Spectrometer (TOMS) and ground-based measurements, J. Geophys. Res., 108, 8238, doi:10.1029/2001JD000967, 2003a. 3236

Thompson, A., Witte, J., Oltmans, S., Schmidlin, F., Logan, J., Fujiwara, M., Kirchhoff, V., Posny, F., Coetzee, G., Hoegger, B., Kawakami, S., Ogawa, T., Fortuin, J., and Kelder, H.: Southern Hemisphere Additional Ozonesondes (SHADOZ) 1998–2000 tropical ozone climatology 2. Tropospheric variability and the zonal wave-one, J. Geophys. Res., 108, D28241, doi:10.1029/2002JD002241, 2003b. 3236

Tie, X. X., Madronich, S., Walters, S., Rasch, P., and Collins, W.: Effect of clouds on photolysis and oxidants in the troposphere, J. Geophys. Res., 108, D204642, doi:10.1029/2003JD003659, 2003. 3218

GMDD
5, 3217–3260, 2012

Voulgarakis, A., Savage, N. H., Wild, O., Carver, G. D., Clemitshaw, K. C., and Pyle, J. A.: Upgrading photolysis in the p-TOMCAT CTM: model evaluation and assessment of the role of clouds, Geosci. Model Dev., 2, 59–72, doi:10.5194/gmd-2-59-2009, 2009. 3218, 3224, 3229

Voulgarakis, A., Telford, P. J., Aghedo, A. M., Braesicke, P., Faluvegi, G., Abraham, N. L., Bowman, K. W., Pyle, J. A., and Shindell, D. T.: Global multi-year O_3-CO correlation patterns from models and TES satellite observations, Atmos. Chem. Phys., 11, 5819–5838, doi:10.5194/acp-11-5819-2011, 2011. 3232, 3234, 3235

Wild, O., Zhu, X., and Prather, M.: Fast-J: accurate simulation of in- and below-cloud photolysis in tropospheric chemical models, J. Atmos. Chem., 37, 245–282, doi:10.1023/A:1006415919030, 2000. 3218, 3222

Yienger, J. and Levy II, H.: Empirical model of global soil biogenic NO_x emissions, J. Geophys. Res., 100, 11477–11464, 1995. 3221

Young, P.: The influence of Biogenic Emissions on Atmospheric Chemistry: a Model Study for Present and Future Atmospheres, PhD thesis, University of Cambridge, http://ulmss-newton.lib.cam.ac.uk/vwebv/holdingsInfo?bibId=30191, 2007. 3220

Zeng, G. and Pyle, J. A.: Changes in tropospheric ozone between 2000 and 2100 modeled in a chemistry-climate model, Geophys. Res. Lett., 30, 1392, 4 pp., doi:10.1029/2002GL016708, 2003. 3220

GMDD

5, 3217–3260, 2012

Table 1. Quantitative assessment of model performance in October 2005 with ERA-Interim nudging using the statistical assessments of Telford et al. (2008) for potential temperature (θ) and zonal wind (u). This calculates the model mean on four representative model levels and determines the root mean squared error (RMSE) and correlations over time (TC) and space (SC) with respect to the ERA-Interim analyses on these same levels.

	Level	Mean and Bias	RMSE	TC	SC
θ	6	285.3 + 0.5 K	2.7 K	0.75	0.98
	16	306.8 + 0.1 K	0.5 K	0.97	1.00
	29	414.9 + 0.1 K	0.6 K	0.99	1.00
	35	608.5 + 0.2 K	1.0 K	0.98	1.00
u	6	$4.19 + 0.01\,\mathrm{m\,s^{-1}}$	$3.37\,\mathrm{m\,s^{-1}}$	0.79	0.91
	16	$7.40 - 0.01\,\mathrm{m\,s^{-1}}$	$1.45\,\mathrm{m\,s^{-1}}$	0.96	0.99
	29	$13.52 - 0.13\,\mathrm{m\,s^{-1}}$	$1.17\,\mathrm{m\,s^{-1}}$	0.97	1.00
	35	$16.19 - 0.22\,\mathrm{m\,s^{-1}}$	$1.37\,\mathrm{m\,s^{-1}}$	0.97	1.00

GMDD
5, 3217–3260, 2012

Table 2. Quantitative comparison between photolysis frequencies from INTEX data and modelled frequencies with interactive and climatological photolysis.

	Climatological			Interactive		
Reaction	Bias (%)	Correl.	RMSD (%)	Bias (%)	Correl.	RMSD (%)
$O_3 \rightarrow O_2 + O(1D)$	−48	0.83	55	0	0.91	15
$NO_2 \rightarrow NO + O(3P)$	−20	0.65	31	2	0.85	18
$CH_3CHO \rightarrow CH_3OO + HO_2 + CO$	115	0.19	135	−13	0.85	44
$CH_3ONO_2 \rightarrow HO_2 + HCHO + NO_2$	−19	−0.03	46	−1	0.88	17
$H_2O_2 \rightarrow OH + OH$	−24	0.70	34	−2	0.88	16
$HCHO \rightarrow HO_2 + HO_2 + CO$	−35	0.82	41	4	0.92	15
$HCHO \rightarrow H_2 + CO$	−31	0.81	39	−4	0.91	16
$HONO \rightarrow OH + NO$	−21	0.66	33	−23	0.83	30
$HO_2NO_2 \rightarrow HO_2 + NO_2$	−22	0.77	31	0	0.88	15
$PAN \rightarrow CH_3CO_3 + NO_2$	−87	0.47	92	12	0.82	23

GMDD
5, 3217–3260, 2012

Table 3. Ozone Budget.

	Prod. $Tgyr^{-1}$	Loss $Tgyr^{-1}$	Dry Dep. $Tgyr^{-1}$	Wet Dep. $Tgyr^{-1}$	STE $Tgyr^{-1}$	Burden Tg	τ_{CH_4} yr
Climatological	4590	3460	1040	120	420	357	9.6
Interactive	5650	4450	1010	130	450	351	6.7
Stevenson et al. (2006)	5110 ± 606	4668 ± 727	1003 ± 200		552 ± 168	344 ± 39	8.67 ± 1.32
Morgenstern et al. (2012)	3865	3451	724		329	296	10.5

GMDD
5, 3217–3260, 2012

Table A1. Photolysis cross sections employed in MetUM Fast-JX.

	Reaction	Notes	Reference
1.	$O_2 \rightarrow O(3P) + O(1D)$	Cross section 0 in Fast-JX wavelengths.	
2.	$O_2 \rightarrow O(3P) + O(3P)$	*T*-dependence between 180 and 300 K.	Prather et al. (2010).
3.	$O_3 \rightarrow O_2 + O(1D)$	*T*-dependence between 180 and 300 K.	Prather et al. (2010).
4.	$O_3 \rightarrow O_2 + O(3P)$	*T*-dependence between 180 and 300 K.	Prather et al. (2010).
5.	$NO \rightarrow N + O(3P)$		Prather et al. (2010).
6.	$NO_2 \rightarrow NO + O(3P)$	*T*-dependence between 220 and 298 K.	Prather et al. (2010).
7.	$NO_3 \rightarrow NO + O_2$	*T*-dependence between 190 and 300 K.	Sander et al. (2006).
8.	$NO_3 \rightarrow NO_2 + O(3P)$	*T*-dependence between 190 and 300 K.	Sander et al. (2006).
9.	$N_2O_5 \rightarrow NO_3 + NO_2$	*T*-dependence between 230 and 300 K.	Sander et al. (2006).
10.	$HONO \rightarrow OH + NO$		Sander et al. (2006).
11.	$HONO_2 \rightarrow OH + NO_2$	*T*-dependence between 200 and 300 K. Includes IR photolysis of Jiménez et al. (2005).	Sander et al. (2006).
12.	$HO_2NO_2 \rightarrow HO_2 + NO_2$	*T*-dependence between 200 and 300 K. Includes IR photolysis of Jiménez et al. (2005).	Sander et al. (2006).
13.	$N_2O \rightarrow N_2 + O(1D)$	*T*-dependence between 200 and 300 K.	Prather et al. (2010).
14.	$H_2O \rightarrow OH + H$		Sander et al. (2006).
15.	$CH_4 \rightarrow CH_3OO + H$	Cross Sect. 0 in Fast-JX wavelengths.	
16.	$CO_2 \rightarrow CO + O(3P)$	*T*-dependence between 195 and 295 K.	Parkinson et al. (2003).
17.	$H_2O_2 \rightarrow OH + OH$	*T*-dependence between 200 and 300 K.	Prather et al. (2010).
18.	$HCHO \rightarrow HO_2 + HO_2 + CO$	*T*-dependence between 223 and 293 K.	Prather et al. (2010).
19.	$HCHO \rightarrow H_2 + CO$	*T*-dependence between 223 and 293 K.	Prather et al. (2010).
20.	$CH_3OOH \rightarrow HO_2 + HCHO + OH$		Sander et al. (2006).
21.	$CH_3CHO \rightarrow CH_3OO + HO_2 + CO$		Sander et al. (2006).
22.	$CH_3CHO \rightarrow CH_4 + CO$		Sander et al. (2006).
23.	$C_2H_5CHO \rightarrow C_2H_5OO + HO_2 + CO$		Sander et al. (2006).
24.	$C_2H_5CHO \rightarrow CH_3OH + HO_2 + OH$		Sander et al. (2006).
25.	$CH_3O_3H \rightarrow CH_3OO + OH$		Sander et al. (2006).
26.	$(CH_3)_2CO \rightarrow CH_3CO3 + CH_3OO$	Using scheme of Blitz et al. (2004).	Prather et al. (2010).
27.	$n-PrOOH \rightarrow C_2H_5CHO + HO_2 + OH$	Use frequencies from reaction 20.	
28.	$i-PrOOH \rightarrow (CH_3)_2CO + HO_2 + OH$	Use frequencies from reaction 20.	
29.	$CH_3COCH_2OOH \rightarrow CH_3CO_3 + HCHO + OH$	Use frequencies from reaction 20.	

GMDD
5, 3217–3260, 2012

Table A1. Continued.

	Reaction	Notes	Reference
30.	HACET → CH_3CO_3 + HCHO + HO_2	Lumped species of C3 carbonyls, including hydroxyacetone. Use hydroxyacetone frequencies.	Sander et al. (2006).
31.	MGLY → CH_3CO_3 + CO + HO_2	Lumped species of C3 aldehydes, including methyl glyoxal. Use methylglyoxal frequencies.	IUPAC datasheet P6[a]
32.	MACR → CH_3CO_3 + HCHO + CO + HO_2	Lumped species of C4 carbonyls, including methacrolein. Use methacrolein frequencies.	Prather et al. (2010).
33.	MACROOH → 0.5HACET + 0.5CO +0.5MGLY + 0.5HCHO + OH + HO_2	Use frequencies from reaction 20.	
34.	iSOOH → MACR + HO_2 + HCHO + OH	Use frequencies from reaction 20.	
35.	CH_3ONO_2 → HO_2 + HCHO + NO_2	*T*-dependence between 240 and 300 K.	Prather et al. (2010).
36.	PAN → CH_3CO_3 + NO_2	*T*-dependence between 250 and 300 K.	Prather et al. (2010).
37.	PPAN → $C_2H_5CO_3$ + NO_2	Use frequencies from reaction 36.	
38.	MPAN → $MACRO_2$ + NO_2	Use frequencies from reaction 36.	
39.	NALD → HCHO + CO + NO_2 + CO_2	Use frequencies from reaction 21.	
40.	ISON → NO_2 + MACR + HCHO + NO_2	Lumped Species. Use i−$C_3H_7ONO_2$ *T*-dependence between 230 and 360 K.	IUPAC datasheet P17[b]
41.	CH_3Br → Br + H	*T*-dependence between 196 and 296 K.	Prather et al. (2010).
42.	BrCl → Br + Cl	*T*-dependence between 190 and 300 K.	Sander et al. (2006).
43.	BrO → Br + O(3P)		Sander et al. (2006).
44.	HOBr → Br + OH		Prather et al. (2010).
45.	$BrNO_3$ → Br + NO_3		Sander et al. (2006).
46.	$BrNO_3$ → BrO + NO_2		Sander et al. (2006).
47.	$CFCl_3$ → Cl + Cl + Cl		Prather et al. (2010).
48.	CF_2Cl_2 → Cl + Cl		Prather et al. (2010).
49.	HCl → H + Cl		Sander et al. (2006).
50.	HOCl → Cl + OH		Prather et al. (2010).
51.	OClO → ClO + O(3P)		Sander et al. (2006).
52.	Cl_2O_2 → Cl + Cl + O_2		Sander et al. (2006).
53.	$ClNO_3$ → Cl + NO_3		Prather et al. (2010).
54.	$ClNO_3$ → ClO + NO_2		Prather et al. (2010).

[a] http://www.iupac-kinetic.ch.cam.ac.uk/datasheets/pdf/P6_CH3COCHO+hv.pdf

[b] http://www.iupac-kinetic.ch.cam.ac.uk/datasheets/pdf/P17_i-C3H7ONO2+hv.pdf

GMDD
5, 3217–3260, 2012

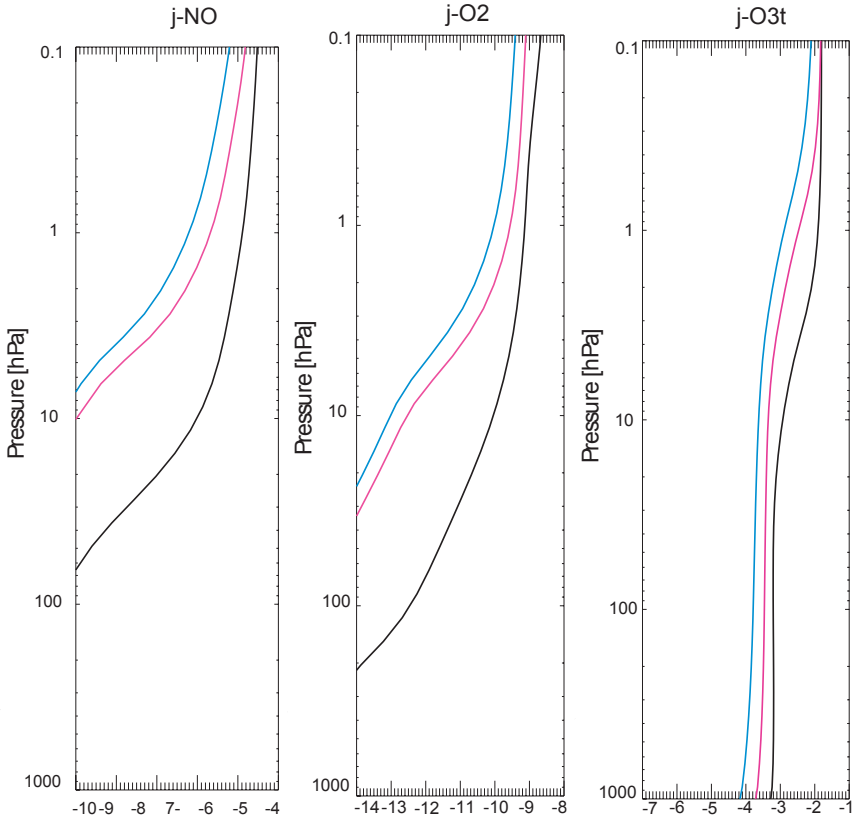

Fig. 1. Photolysis frequencies for the CCMVal photolysis assessment scenarios for NO (left), O_2 (centre) and O_3 (right). The three lines correspond to a solar zenith angle of 15° (black), 84° (pink) and averaged over a day between 84° and 96° (blue). This figure can be compared to Fig. 6.1 in Chipperfield et al. (2010).

GMDD
5, 3217–3260, 2012

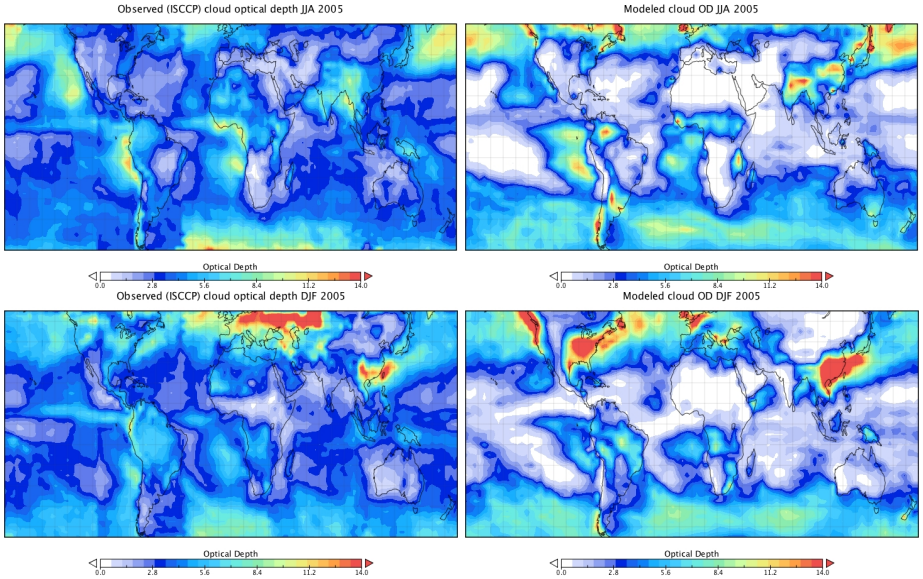

Fig. 2. Average cloud optical depth from ISCCP satellite data (left) and the UM (right). The top row contains a comparison for the Northern Hemisphere winter season and the bottom row for the summer season.

GMDD
5, 3217–3260, 2012

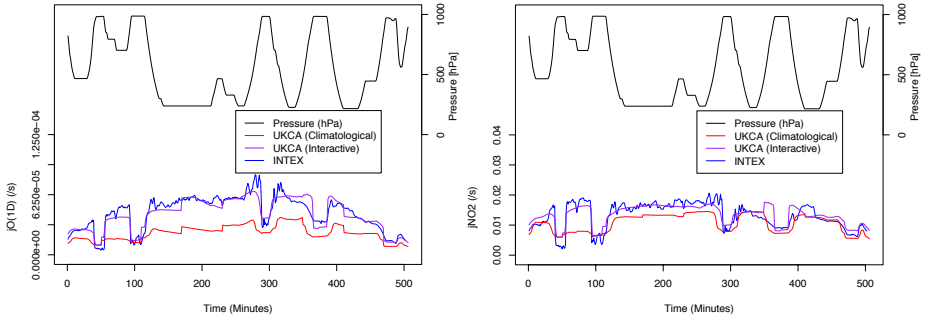

Fig. 3. Comparison of $O_3 \rightarrow O(^1D)$ (top) and NO_2 (bottom) photolysis frequencies during the first flight (1 July 2004) in the INTEX-NA campaign between observations and the model with climatological and interactive photolysis frequencies.

GMDD
5, 3217–3260, 2012

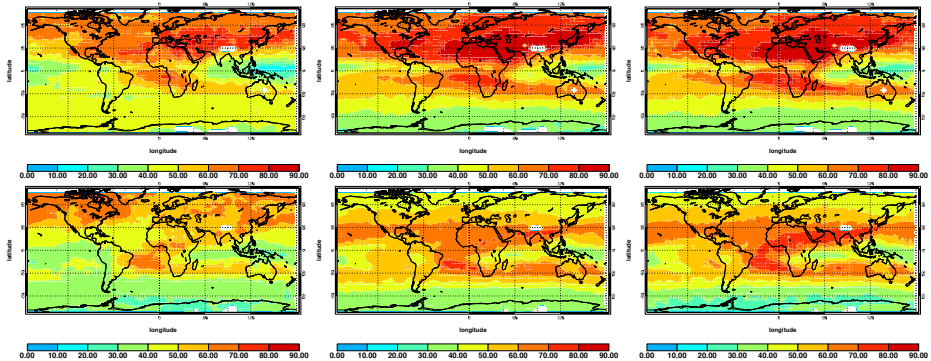

Fig. 4. Ozone [ppbv] averaged over 800–400 hPa from 2005–2008 July/August (top row) and Dec/Jan (bottom row). Left column: observations from TES. Middle column: model with climatological photolysis. Right column: model with interactive photolysis.

GMDD
5, 3217–3260, 2012

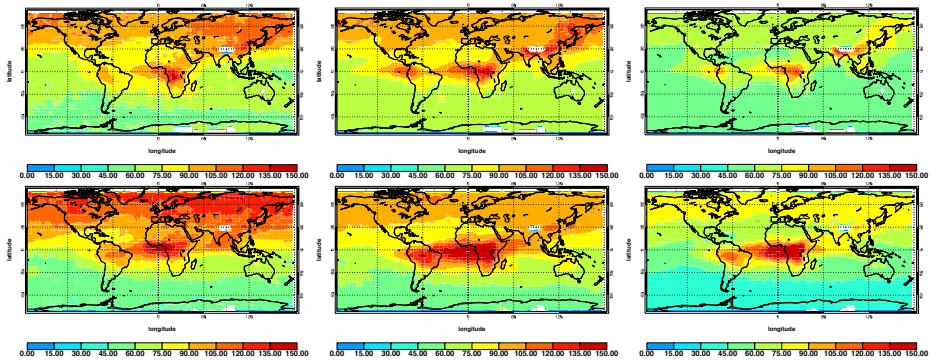

Fig. 5. Carbon Monoxide (ppbv) averaged over 800–400 hPa from 2005–2008 July/August (top row) and December/January (bottom row). Left column: observations from TES. Middle column: model with climatological photolysis. Right column: model with interactive photolysis.

GMDD
5, 3217–3260, 2012

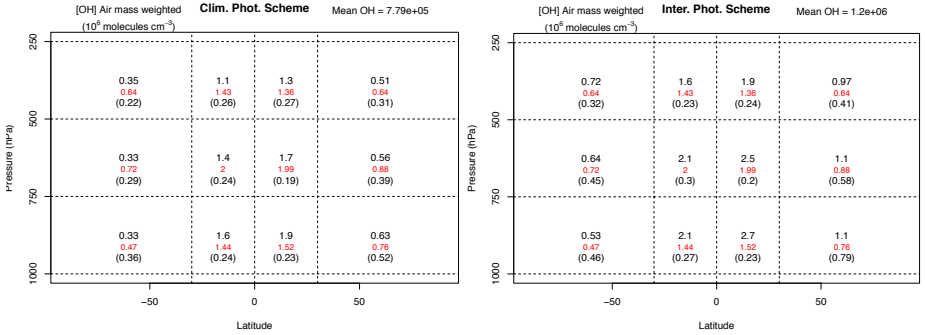

Fig. 6. OH distribution, weighted as in (Lawrence et al., 2001), as a function of height and latitude. The black numbers are the model values, the red numbers are from the Spivakovsky et al. (2000) climatology (obtained from Lamarque et al., 2012) and the numbers in brackets the standard deviation of the model. Top plot with climatological photolysis and bottom plot with interactive photolysis.

GMDD
5, 3217–3260, 2012

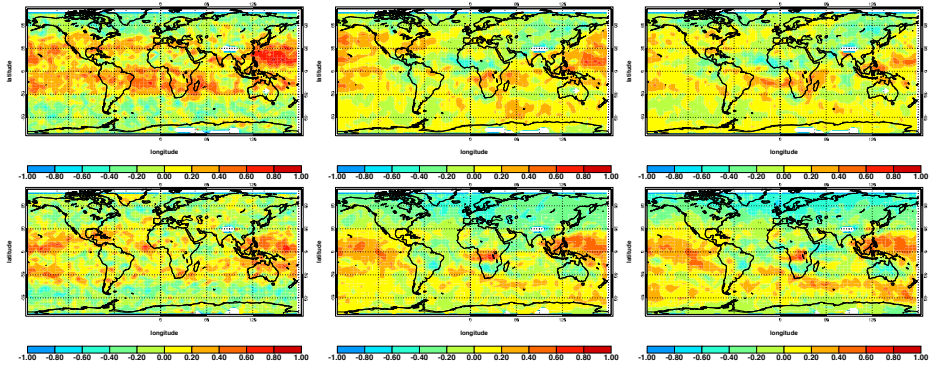

Fig. 7. Correlation between "free tropospheric" (800–400 hPa) Ozone and Carbon Monoxide from 2005–2008 July/August (top row) and December/January (bottom row). Left column: observations from TES. Middle column: model with climatological photolysis. Right column: model with interactive photolysis.

GMDD
5, 3217–3260, 2012

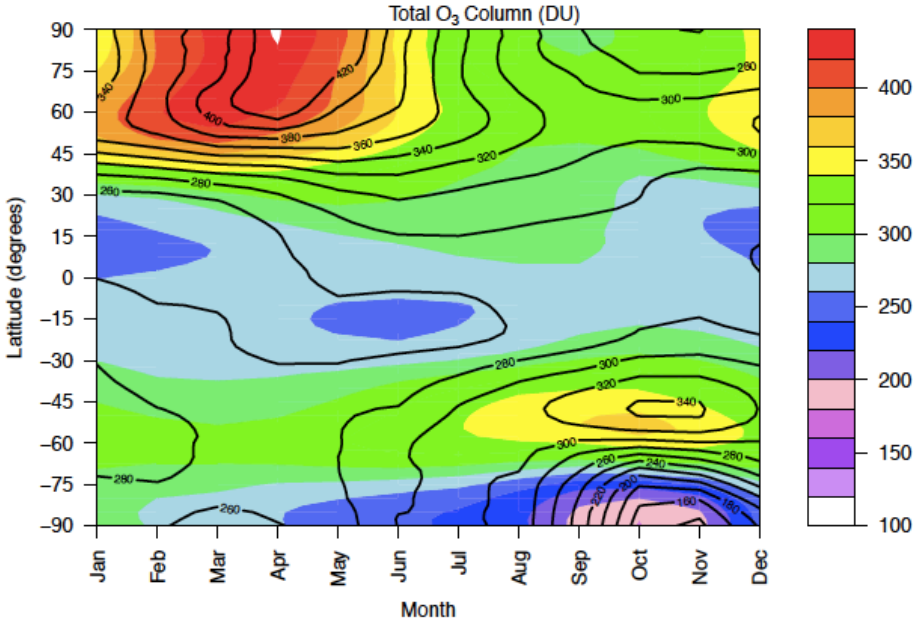

Fig. 8. Comparison of O_3 column between assimilated total ozone column data (Bodeker et al., 2005) (lines) and the stratospheric chemistry model (filled coloured contours).

GMDD
5, 3217–3260, 2012

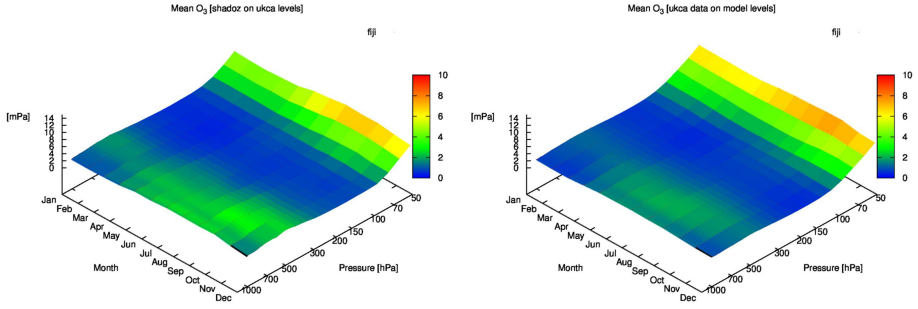

Fig. 9. Comparison of monthly mean O_3 profiles between the stratospheric version of the chemistry model and sondes from the SHADOZ network over an example site, in this case Fiji.

GMDD
5, 3217–3260, 2012